ARTICLE

BIOTECHNOLOGY and BIOENGINEERING

Modeling Electrostatic Exclusion Effects During Ion Exchange Chromatography of Monoclonal Antibodies

Andrew L. Zydney,[1] Chithkala Harinarayan,[2] Robert van Reis[2]

[1]Department of Chemical Engineering, The Pennsylvania State University, University Park, Pennsylvania 16802; telephone: 814-863-7113; fax: 814-865-7846; e-mail: zydney@engr.psu.edu

[2]Genentech, Inc., South San Francisco, California

Received 28 May 2008; revision received 22 July 2008; accepted 25 July 2008

Published online 19 September 2008 in Wiley InterScience (www.interscience.wiley.com). DOI 10.1002/bit.22145

ABSTRACT: Recent experimental studies have shown a reduction in dynamic- binding capacity for both monoclonal antibodies and antigen-binding fragments at very low conductivity, conditions that should generate the greatest electrostatic attraction. This behavior has been attributed to the steric and electrostatic exclusion of the charged protein from the entrance of the resin pores. This manuscript presents a quantitative mathematical description of this phenomenon. The protein partition coefficient was evaluated using models for the partitioning of a charged sphere into a charged cylindrical pore, with the pore size distribution evaluated by inverse size exclusion chromatography. The results were in very good agreement with experimental data for batch protein uptake and dynamic-binding capacity over a range of pH and conductivity. This theoretical framework provides important insights into the behavior of ion exchange chromatography for protein purification.

Biotechnol. Bioeng. 2009;102: 1131–1140.

KEYWORDS: chromatography; ion exchange; electrostatics; antibody; protein

Introduction

Recent studies of dynamic-binding capacities for several monoclonal antibodies in SP Sepharose™ XL and SP Sepharose Fast Flow cation exchange resins showed a significant reduction in dynamic-binding capacity at very low ionic strength and low pH (Harinarayan et al., 2006) conditions that would have been expected to generate the greatest electrostatic attraction between the positively charged proteins and the negatively charged resin. Confocal scanning laser microscopy demonstrated that this reduction in dynamic-capacity was caused by a dramatic reduction in mass transfer rates within the porous cation exchange particles, with the antibodies penetrating only a few microns into the particle interior under low ionic strength conditions. Harinarayan et al. (2006) hypothesized that this reduction in dynamic-binding capacity was due to an electrostatic and steric exclusion mechanism, with the initial binding of the charged protein to the outer region of the pores hindering subsequent transport of charged proteins into the pores.

Similar results were reported by Faude et al. (2007) for the dynamic-binding capacity of two different monoclonal antibodies on a series of cation exchange resins (Fractogel EMD, SP Sepharose XL, and Toyopearl Prototype S). In all cases, there was a distinct maximum in the dynamic-binding capacity at intermediate pH (or conductivity), with the location of this maximum well correlated with the protein zeta potential. Data obtained by Ljunglöf et al. (2007) using an antigen-binding antibody fragment (Fab) also show a maximum in dynamic-binding capacity at intermediate conductivity, although only at low pH, suggesting that this behavior may hold for a range of proteins.

Previous studies of mass transfer within ion exchange chromatography particles have generally focused on a combination of pore (solution) and surface diffusion. Several studies have hypothesized that electrokinetic effects may also be important, leading to a "hump" in the radial concentration profile, and in turn a "concentration overshoot" for some experimental conditions (Dziennik et al., 2003; Grimes and Liapis, 2002; Hubbuch et al., 2003). However, more recent work by Teske et al. (2006) has demonstrated that this overshoot is an experimental artifact associated with the different adsorptive behavior of the labeled and non-labeled protein. In addition, none of the theoretical analyses has predicted the dramatic reduction in

Correspondence to: A.L. Zydney

the rate of protein mass transfer into the particle at low conductivity and low pH observed by Harinarayan et al. (2006) and Faude et al. (2007).

Direct measurements of protein diffusion in charged agarose gels (Johnson et al., 1995) have demonstrated that the protein mobility is largely unaffected by pH and ionic strength, but the equilibrium partition coefficient between the gel and free solution is significantly reduced by electrostatic repulsion between the like-polarity protein and gel. This effect was most pronounced at low ionic strength due to the reduction in electrostatic shielding under these conditions. Similar effects have been reported by Zhang and Sun (2002) for diffusion of negatively charged albumin molecules within the pores of a Sepharose resin that was modified by covalent attachment of a negatively charged dye-ligand (Cibacron Blue 3GA). Zhang and Sun (2002) hypothesized that the observed reduction in protein diffusion coefficient at low ionic strength was due to the reduction in the effective pore diameter associated with the increased thickness of the electrical double layer, although no quantitative analysis of this phenomenon was presented.

More recently, Stone and Carta (2007) evaluated an effective protein diffusion coefficient in dextran-grafted SP-matrix based on fitting transient protein uptake data to a simple mass transfer model. The calculated values of the effective lysozyme diffusivity in the dextran-grafted SP-matrix were greater than those in free solution, which the authors attributed to either a solid-phase diffusion mechanism facilitated by the flexibility of the dextran chains or to a non-diffusive mechanism associated with the electrostatic potential. No quantitative analysis of these mechanisms was presented, nor was there any independent data for the underlying phenomena.

Harinarayan et al. (2006) attributed the "exclusion mechanism" in the cation exchange resins to a steric and electrostatic repulsion that developed because the effective charge of the cation exchanger became positive, that is, of the same polarity as the protein, at the high levels of adsorption of the positively charged antibody at the outer region of the particle. This type of "charge reversal" has been reported previously by Yamamoto et al. (1992) for carboxymethyl Sephadex C-25 particles, with the zeta potential of the negatively charged particles becoming positive (as measured by microelectrophoresis) after adsorption of positively charged lysozyme. Similar effects have been seen by Yamaguchi et al. (1996) using negatively charged dextran sulfate polymers, which formed a positively charged complex with lysozyme (as determined from the measured electrophoretic mobility). However, the possible effect of such charge reversal on protein transport has never been investigated.

The objective of this study was to develop a quantitative mathematical description of antibody uptake and dynamic-binding capacity in Sepharose XL cation exchange particles incorporating both steric and electrostatic exclusion effects at the pore entrance. The protein partition coefficient into the resin was evaluated using the model developed by Smith and Deen (1980) for the partitioning of a charged sphere into a charged cylindrical pore, a theoretical framework that has been used very effectively to describe electrostatic exclusion effects for proteins in both ultrafiltration membranes (Burns and Zydney, 2001; Pujar and Zydney, 1994) and size exclusion chromatography resins (Pujar and Zydney, 1998). The pore size distribution within the Sepharose XL particles was determined by inverse size exclusion chromatography using a series of dextran standards. Model calculations were compared with experimental data for protein transport into the porous resin obtained by confocal scanning laser microscopy and traditional batch uptake experiments. The dynamic-binding capacity was then evaluated using a simple model that incorporates these electrostatic exclusion effects, with the results in very good agreement with recent experimental data obtained by Harinarayan et al. (2006).

Theoretical Development

The dynamic-binding capacity was evaluated using a simple model for protein diffusion into the porous cation exchange particles accounting for electrostatic exclusion effects at the pore entrance. Each particle was assumed to consist of an array of non-interconnected cylindrical pores. The local one-dimensional protein diffusive flux within each pore is:

$$J_D = -K_D D_\infty \frac{\partial C}{\partial z} \tag{1}$$

where C is the local protein concentration within the pore and D_∞ is the free solution diffusion coefficient. K_D is the hindrance factor for diffusion and accounts for the additional hydrodynamic drag on the protein due to the presence of the pore walls. Bungay and Brenner (1973) evaluated K_D for the transport of an uncharged sphere in an uncharged cylindrical pore with the results expressed as:

$$K_D = \frac{K_s}{2K_t} \tag{2}$$

where K_s and K_t are expressed as expansions in $\lambda = r_s/r$:

$$\begin{bmatrix} K_t \\ K_s \end{bmatrix} = \frac{9}{4}\pi^2\sqrt{2}(1-\lambda)^{-5/2} \times \left[1 + \sum_{n=1}^{2}\begin{pmatrix} a_n \\ b_n \end{pmatrix}(1-\lambda)^n\right] + \sum_{n=0}^{4}\begin{pmatrix} a_{n+3} \\ b_{n+3} \end{pmatrix}\lambda^n \tag{3}$$

with r_s and r the protein and pore radius, respectively. The coefficients a_n and b_n are given in Bungay and Brenner (1973). Pujar and Zydney (1997) have shown that electrostatic interactions with the pore wall have relatively

little effect on the hindrance factor for diffusion, in good agreement with experimental results by Johnson et al. (1995).

Equation (1) was integrated over the (sharp) penetration distance, L(t), in each pore assuming quasi-steady behavior giving:

$$J_D = \frac{\phi K_D D_\infty C_\infty}{L(t)} \tag{4}$$

where C_∞ is the protein concentration in the external solution. Note that Equation (4) ignores the spherical geometry of the resin particles since the model is based on diffusion through a pore of uniform cross-sectional area. The equilibrium partition coefficient (ϕ) for the protein between the pore and the external solution is evaluated as:

$$\phi = (1-\lambda)^2 \exp\left(-\frac{\psi_E}{kT}\right) \tag{5}$$

The first term in Equation (5) accounts for the steric exclusion of the protein from the region within one protein radius of the pore walls, while the second term accounts for the electrostatic energy of interaction between the protein and the pore wall. Smith and Deen (1980) evaluated the electrostatic energy of interaction by solving the linearized Poisson–Boltzman equation. The results are expressed as the sum of three terms:

$$\Psi_E = A_{pore}\sigma_{pore}^2 + A_{protein}\sigma_{protein}^2 + A_{p\text{-}s}\sigma_{pore}\sigma_{protein} \tag{6}$$

where σ_{pore} and $\sigma_{protein}$ are the surface charge density of the pore wall and protein, respectively, and A_{pore}, $A_{protein}$, and A_{p-s} are all positive coefficients that depend upon the solution ionic strength, the pore radius, and the protein radius (Smith and Deen, 1980). The first two contributions to the total energy of interaction arise from the deformation of the electrical double layer adjacent to the pore wall and the protein, respectively. These interactions always increase the total free energy of the system, leading to a reduction in the partition coefficient. The final term in Equation (6) is associated with direct charge–charge interactions between the protein and pore wall and can be attractive or repulsive depending upon the polarities. Equations (5) and (6) have been very successfully employed to describe protein partitioning into charged membranes (Burns and Zydney, 2001; Mehta and Zydney, 2006; Pujar and Zydney, 1994).

A simple one-dimensional mass balance was used to describe the rate of penetration of the protein front into the cylindrical pore:

$$q_p 2\pi r \frac{dL}{dt} = \pi (r - d_{ads})^2 J_D \tag{7}$$

where d_{ads} is the thickness of the adsorbed layer of protein within the pore and q_p is the surface coverage of adsorbed protein (in kg/m^2). Equation (4) is substituted into Equation (7), with the resulting expression integrated over time to give:

$$L(t) = \sqrt{\frac{\phi K_D D_\infty C_\infty (r - d_{ads})^2 t}{q_p r}} \tag{8}$$

Equation (8) is valid for $L < R$ where R is the radius of the cation exchange particles, assumed to be equal to the maximum length of an individual pore within the spherical resin particle.

In order to account for the presence of a pore size distribution within the resin particles, the average fractional penetration of the protein into the pore was evaluated by integrating Equation (8) over the pore size distribution:

$$f_{uptake} = \frac{\int r^2 f_R(r) L(t)\, dr}{\int r^2 f_R(r) R\, dr} \tag{9}$$

where R is the radius of the resin particles and the weighting by r^2 in both the numerator and dominator accounts for the dependence of the pore volume on the radius. The integrals in Equation (9) were only performed over pore radii that were large enough to accommodate the protein, that is, for $r - d_{ads} > r_{protein}$. All calculations were done assuming a log-normal distribution (Zydney et al., 1994):

$$f_R(r) = \frac{1}{r\sqrt{2\pi}}\left[\ln\left(1+\frac{\sigma}{\bar{r}}\right)^2\right]^{-1/2} \times \exp\left(-\frac{\left(\ln(r/\bar{r})[1+(\sigma/\bar{r})^2]^{1/2}\right)^2}{2\ln[1+(\sigma/\bar{r})^2]}\right) \tag{10}$$

where $\bar{r}$ and σ are the mean and standard deviation of the distribution. The log-normal pore size distribution is particularly convenient for this type of analysis since it is only defined for positive values of r (in contrast to the standard normal or Gaussian distribution which goes from negative to positive infinity).

The surface charge density of the monoclonal antibody was evaluated from its amino acid sequence, yielding $Z = 107$, 57, and 35 at pH 4, 5, and 6, respectively (Harinarayan et al., 2006), with the surface area of the protein evaluated from the dimensions of a typical immunoglobulin as 174 nm^2 (de la Torre and Carrasco, 2002). The surface charge density of the resin, after adsorption of protein, was evaluated as the weighted sum of the charge density of both the adsorbed protein and the base resin using a simple linear superposition:

$$\sigma_{pore} = q_{protein}\left(\frac{V}{A}\right)\left(\frac{Z}{m_p}\right) + \beta\sigma_{resin} \tag{11}$$

where $q_{protein}$ is the protein uptake (in mass per volume) in the region occupied by the penetrating front, A/V is the area per unit volume for the resin (determined from the pore size distribution), and Z/m_p is the charge per unit mass for the protein. Equation (11) implicitly assumes that some fraction of the resin charge was "visible" through the adsorbed protein layer. The surface charge density of the base resin was evaluated from the ion exchange capacity (on a per volume basis) and the calculated surface area (using the previously determined values for the mean pore size and the standard deviation in the log-normal distribution). The parameter β was fit to the experimental data by minimizing the sum of the squared residuals between the model calculations and experimental data for the fractional uptake.

Materials and Methods

All experiments employed SP Sepharose™ XL (SP XL), a dextran-grafted Sepharose cation exchange resin provided by Amersham Biosciences (now GE Healthcare, Uppsala, Sweden). Protein uptake and dynamic-binding capacity experiments were performed with a full-length monoclonal antibody provided by Genentech Inc. (South San Francisco, CA).

Batch Uptake Measurements

Protein uptake by isolated resin was evaluated as follows: 20 mL of an 8 mg/mL solution of the monoclonal antibody was added to a reaction vessel equipped with a hanging stirrer. The reaction vessel was connected to a Multitemp II water bath (GE Healthcare), the temperature was set to 21°C, and a defined amount of resin (settled gel diluted 1:2 with buffer) was added to the stirred protein solution. Samples were taken directly from the reaction vessel at fixed times, with the protein concentration evaluated by UV. Protein uptake at any time t was evaluated as:

$$Q = \frac{V_M(C_0 - C)}{V_s} \tag{12}$$

where V_M is the volume of mobile phase, V_s is the volume of the solid-phase, and C_0 and C are the protein concentrations in the initial solution and at time t.

Inverse Size Exclusion Chromatography

The pore size distribution of the SP XL resin was estimated using inverse size exclusion chromatography following an approach similar to that used by Stone and Carta (2007). Dextrans with relatively narrow molecular weight distributions were obtained from TdB Consultancy Inc. (Uppsala, Sweden). Data were obtained using neutral dextrans with nominal molecular mass of 1, 10, 40, 110, 500, 800, and 2,000 kDa, corresponding to viscosity radii of 0.87, 2.71, 5.16, 8.35, 17.71, 22.23, and 37.23 nm. Additional experiments were performed with negatively charged dextran propylsulfonate.

Each dextran was dissolved in the appropriate buffer at a concentration of approximately 1 mg/mL. Peak retention volumes were evaluated using columns having packed bed volumes of 60 mL, bed diameters of 1.6 cm, and bed heights of 30 cm (XK16/30, GE Healthcare). Dextran detection was by refractive index (RI 72, Shodex, Kawasaki, Japan). The dextran distribution coefficient, which is approximately equal to the average equilibrium partition coefficient between the bulk solution and the pore volume, was evaluated as:

$$\overline{\phi} = \frac{V_r - V_0}{V_t - V_o} \tag{13}$$

where V_r is the peak retention volume for the dextran of given radius, V_0 is the excluded or void volume (calculated using the 2,000 kDa dextran), and V_t is the total liquid volume of the column (calculated using data for glucose).

Dynamic-Binding Capacity

Dynamic-binding capacity experiments were performed on an AKTA Explorer 100 (Amersham Biosciences) using columns with a packed bed volume of 3.4 mL. All experiments were performed at ambient room temperature (25–27°C) at a linear velocity of 100 cm/h. Data were obtained at pH 4 and 5 using a 15 mM sodium acetate buffer (Fisher Scientific, Hampton, NH), with the pH adjusted using glacial acetic acid (Mallinckrodt, Phillipsburg, NJ) and the conductivity adjusted using NaCl. Data at pH 6 used 14 mM MES [2-(N-morpholino)ethanesulfonic acid] and 10 mM MES Sodium salt (Angus Buffers and Biochemicals, Buffalo Grove, IL), with the pH adjusted using 50% NaOH (J.T. Baker). The resins were initially equilibrated with the load buffer, and the protein was loaded onto the resin to 10% breakthrough capacity based on the absorbance at 280 nm. Experiments were performed in triplicate, with results reported as the average value.

A more detailed discussion of many of the experimental procedures is provided by Harinarayan et al. (2006).

Results and Analysis

Resin Characterization

The mean and standard deviation in the log-normal pore size distribution were estimated using inverse size exclusion chromatography based on the measured values of the partition coefficient for the neutral dextrans in the accessible pores of the dextran-grafted Sepharose cation exchange resin. Results for two repeat experiments performed at a solution conductivity of 50 mS/cm (corresponding to an ionic strength of approximately 550 mM) are shown in the

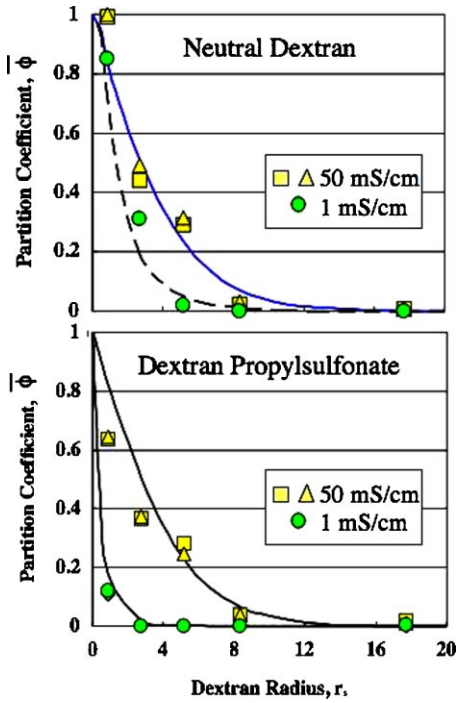

Figure 1. Partition coefficient in the SP XL resin determined from a size exclusion chromatography experiment using neutral (top panel) and negatively charged (bottom panel) dextrans. Solid and dashed curves are model calculations as described in the text. [Color figure can be seen in the online version of this article, available at www.interscience.wiley.com.]

top panel of Figure 1, with the data plotted as a function of the dextran viscosity radius determined using the correlation presented by Hagel (1988). The data show a high degree of reproducibility, with the partition coefficients for the two experiments all within 0.05 for a given dextran.

The solid curve in Figure 1 represents the calculated values of the equilibrium partition coefficient determined by integrating over the pore size distribution:

$$\overline{\phi} = \frac{\int r^2 f_R(r)\phi \, dr}{\int r^2 f_R(r) \, dr} \tag{14}$$

where the r^2 in the numerator and denominator accounts for the dependence of the pore volume on r and ϕ is the partition coefficient for a pore of radius r as given by Equation (5). Although the dextrans are electrically neutral, the partition coefficient was evaluated using the full expression for ϕ to account for the small electrostatic exclusion arising from the energetic penalty associated with the distortion of the electrical double layer within the pore (the first term in Eq. 6). The surface charge density of the pore (σ_{pore}) was evaluated from the charge on the native resin:

$$\sigma_{resin} = \frac{I_{resin} F}{\varepsilon_{resin}(A_{pore}/V_{pore})} \tag{15}$$

where I_{resin} is the ionic capacity of the resin (in moles per unit volume), F is the Faraday constant, and ε_{resin} is the porosity of the resin particles. The surface area to volume ratio for the porous resin (A_{pore}/V_{pore}) was evaluated by integration over the pore size distribution.

The best-fit values of the mean pore radius ($\overline{r} = 8.1$ nm) and the standard deviation ($\sigma/\overline{r} = 0.38$) in the log-normal distribution were determined by minimizing the sum of the squared residuals between the data and model calculations. The model properly captures the reduction in partition coefficient with increasing dextran size, with the calculations in very good agreement with the experimental data. It was not possible to obtain an accurate fit to the partition coefficient data using a single pore size (corresponding to $\sigma/\overline{r} = 0$).

The filled circles in the upper panel of Figure 1 represent experimental results for the dextran partition coefficients at low conductivity (1.2 mS/cm, corresponding to an ionic strength of approximately 13 mM). The partition coefficients at low conductivity were uniformly smaller than those at high conductivity. This effect was particularly pronounced for the 30 kDa dextran ($r_s = 5.2$ nm), with the partition coefficient at low conductivity ($\overline{\phi} = 0.021$) being more than an order of magnitude smaller than that at high conductivity ($\overline{\phi} \approx 0.21$). The dashed curve in Figure 1 represents the predicted values of the partition coefficients at low conductivity accounting for the energetic penalty associated with the distortion of the electrical double layer within the pores by the neutral dextrans (the first term in Eq. 6). The model is in good agreement with the experimental data using the same values of the mean and standard deviation in the pore size distribution as determined from the data at high conductivity. Note that Stone and Carta (2007) observed a similar reduction in dextran partition coefficients at low conductivity in an SP-agarose-dextran composite, but they attributed this to a change in morphology of the dextran grafts with changing ionic strength. However, Stone and Carta (2007) evaluated the effective pore size of the resin based on purely steric interactions, ignoring the effects of electrostatic interactions on the partition coefficient. The good agreement between the dextran partition coefficient data and model at both low and high ionic strength using the same pore size distribution suggests that the effective pore size in the SP XL resin (as determined by inverse size exclusion chromatography) is unaffected by solution ionic strength.

In order to validate the electrostatic contributions to the partitioning model, experiments were performed with negatively charged dextran propylsulfonate at both low (1 mS/cm) and high (50 mS/cm) conductivities, with the results shown in the bottom panel of Figure 1. The data at high conductivity are only slightly smaller than the results for the neutral dextrans, consistent with the high degree of electrostatic shielding in the high ionic strength solution. The partition coefficients for the dextran propylsulfonate at low conductivity are significantly smaller than the values in the high conductivity solution reflecting the strong

electrostatic exclusion from the charged pores of the Sepharose XL resin.

The solid curves in the bottom panel of Figure 1 are true model predictions for the partition coefficient of the negatively charged dextran propylsulfonate using the pore size distribution parameters determined from the data for the neutral dextrans. The surface charge density of the dextran propylsulfonate was evaluated based on the degree of substitution, which was approximately 1 in every 3.5 glucose monomers for the dextran propylsulfonate used in these experiments. The model predictions are in excellent agreement with the data at both low and high conductivity, properly capturing the strong electrostatic exclusion of the dextran propylsulfonate from the negatively charged, dextran polymer filled, pores. These results provide further confirmation that the effective pore size distribution can be assumed to be independent of solution ionic strength, at least in the context of solute partitioning.

Batch Uptake

Experimental data for the batch uptake of the monoclonal antibody at pH 5 and a conductivity of 5 mS/cm are shown in Figure 2. The data are presented as the fractional uptake, defined as the uptake evaluated in the batch experiments at any given time divided by the equilibrium uptake determined in a separate set of experiments using a very long adsorption time (typically 7 days). Protein uptake by the SP XL resin is relatively slow under these conditions, with $f \leq 0.7$ over 3,600 s. The slow uptake is consistent with direct observations of the penetration of fluorescently labeled antibody into the SP XL resin obtained using confocal laser scanning microscopy (Harinarayan et al., 2006).

The solid curves in Figure 2 are model calculations using several different values of the parameter β, which describes the contribution of the base resin to the effective surface charge density of the pore wall after protein adsorption (Eq. 11). The fractional uptake was evaluated theoretically using Equations (8)–(10), with the mean and standard deviation for the log-normal distribution taken from the best-fit values determined from the dextran partition coefficient data (Fig. 1). The partition coefficient for the protein was evaluated using Equations (5) and (6) with the surface charge density of the pore given by Equation (11). The values of the key model parameters are summarized in Table I. The results are very sensitive to the value of β. When β is small, the surface charge density on the pore wall is dominated by the charge on the protein, giving rise to strong electrostatic repulsion between the positively charged antibody and the positively charged pore. As β increases, the negative charge on the resin becomes more important, reducing the electrostatic repulsion, eventually leading to an attractive electrostatic interaction and a very rapid uptake of protein. The model calculations with $\beta = 0.44$ are in very good agreement with the experimental data, properly capturing the relatively slow protein uptake caused by the reduction in the protein partition coefficient (ϕ) associated with the electrostatic exclusion of the protein from the pores.

The effect of the solution conductivity on the protein uptake is shown in Figure 3. The fractional uptake increases with increasing solution conductivity due to the reduction in electrostatic interactions at the higher salt concentrations. This effect is quite dramatic, with the fractional uptake at $t = 300$ s increasing from $f = 0.10$ for the 1 mS/cm solution to $f = 0.81$ for the 15 mS/cm solution.

The solid curves in Figure 3 are the model calculations using $\beta = 0.44$ for all values of the solution conductivity. The model is in fairly good agreement with the data for the higher conductivity solutions, properly describing the increase in uptake with increasing solution conductivity. In addition, the model calculations are in very good agreement with the measured protein profiles within individual resin particles as determined by confocal microscopy (Harinarayan et al., 2006). The model does predict significantly lower uptake values for the experiment at 1 mS/cm conductivity. This could be due to an over-estimation of the electrostatic

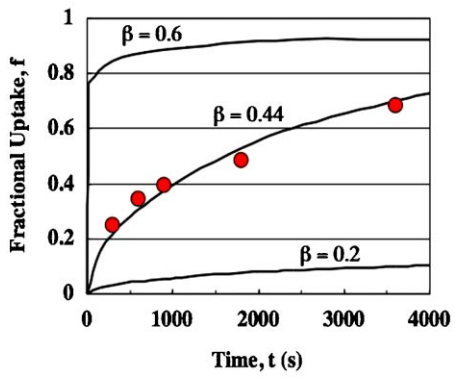

Figure 2. Fractional uptake of a monoclonal antibody as a function of time for the SP XL resin at pH 5 and 5 mS/cm conductivity. Solid curves are model calculations for different values of β. [Color figure can be seen in the online version of this article, available at www.interscience.wiley.com.]

Table I. Physical parameters for model calculations.

Property	Variable	Value
Mean pore radius	$\bar{r}$	8.1 nm
Standard deviation in pore radius	σ	3.1 nm
Resin charge density	σ_{pore}	0.0051 C/m^2
Radius of resin particles	L_{max}	45 μm
Protein radius	r_s	4.8 nm
Protein diffusion coefficient	D_∞	4.5×10^{-11} m^2/s
Protein charge density		
pH 4	$\sigma_{protein}$	0.098 C/m^2
pH 5	$\sigma_{protein}$	0.052 C/m^2
pH 6	$\sigma_{protein}$	0.032 C/m^2
Bed porosity	ε	0.3
Bed height	h	0.1 m
Superficial fluid velocity	u_0	1 m/h

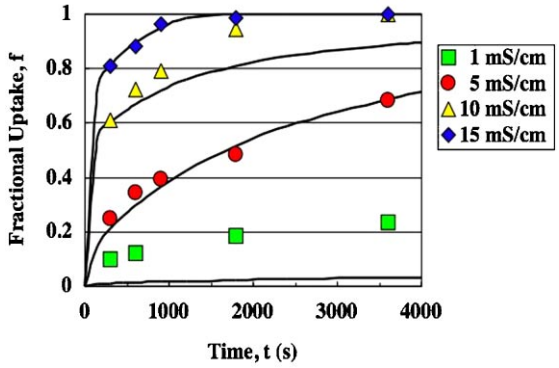

Figure 3. Fractional uptake of a monoclonal antibody as a function of time for the SP XL resin at pH 5 and conductivities of 1, 5, 10, and 15 mS/cm. Solid curves are model calculations with $\beta = 0.44$. [Color figure can be seen in the online version of this article, available at www.interscience.wiley.com.]

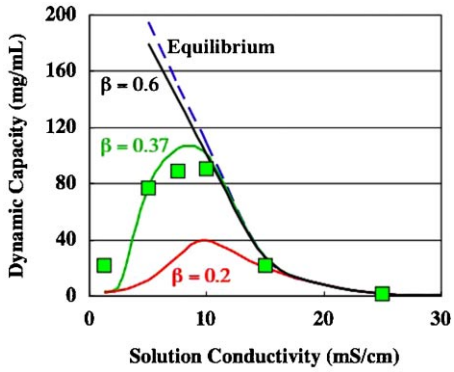

Figure 4. Dynamic-binding capacity of a monoclonal antibody as a function of solution conductivity at pH 5. Solid curves are model calculations for different values of β. [Color figure can be seen in the online version of this article, available at www.interscience.wiley.com.]

repulsion at very low ionic strengths, possibly associated with the use of the linearized form of the Poisson–Boltzmann equation to evaluate the partition coefficient, an approximation that breaks down at very low ionic strength due to the high electrical potential under these conditions. Alternatively, this behavior could reflect the reduction in electrostatic interactions caused by charge regulation effects, a phenomenon that has been discussed previously by Pujar and Zydney (1998) in the context of protein partitioning in porous membranes. In addition, the model completely neglects the dynamic nature of the charged dextrans in the SP XL resin, which could alter the effective pore size and/or give rise to novel transport mechanisms associated with electrostatic potential gradients within the pores (Liapis et al., 2001; Stone and Carta, 2007).

Dynamic-Binding Capacity

The effect of solution conductivity on the dynamic-binding capacity of the monoclonal antibody to the SP XL resin at pH 5 is shown in Figure 4. The dynamic-binding capacity initially increases with increasing conductivity, passing through a maximum at a conductivity of about 10 mS/cm before decreasing to nearly zero at higher conductivities. This behavior has been discussed in some detail by Harinarayan et al. (2006). The reduction in dynamic-binding capacity at high conductivities parallels the reduction in equilibrium (static) binding capacity and is due to the loss of capacity associated with the shielding of the binding interactions at very high salt. The behavior at low conductivities is anomalous—the dynamic-binding capacity decreases even though the attractive (binding) interactions should be enhanced at low conductivities. This behavior is also opposite that seen with the equilibrium uptake, shown by the dashed curve in Figure 4, which increases to more than 200 mg/mL at low conductivity.

The solid curves in Figure 4 are model calculations developed by extending the pore diffusion model to describe the dynamic-binding capacity in a column. It was not possible to evaluate the dynamic-binding capacity using any of the published models for mass transfer in column chromatography since these models do not account for the variation in protein uptake (i.e., penetration distance) over the pore size distribution. Instead, the dynamic-binding capacity was evaluated using a simple mass balance over the column at breakthrough:

$$u_0 A C_b t = [Ah\varepsilon C_b + Ah(1-\varepsilon) q_{eq} f] \qquad (16)$$

where u_0 is the superficial fluid velocity, ε is the bed porosity, h is the bed height, and q_{eq} is the equilibrium (static) protein uptake under the particular experimental conditions. The left-hand side is simply the mass of protein that enters the column over a period t, while the two terms on the right-hand side account for the protein present in the liquid and solid phases within the column. The fractional uptake of protein by the resin particles (f) was evaluated using the same penetration model used to describe the batch uptake; this is equivalent to assuming that all particles within the column are exposed to the bulk protein concentration over the entire experiment. The breakthrough time and dynamic-binding capacity were evaluated by iteratively solving Equation (16). Although this is clearly an approximate analysis, neglecting the detailed shape of the breakthrough curve as well as the progression of the concentration front through the column, the resulting model calculations should provide an appropriate framework for examining the effects of electrostatic exclusion on dynamic-binding capacity.

The solid curves in Figure 4 are model calculations for the dynamic-binding capacity with the pore size distribution evaluated from the dextran partition coefficient data (Fig. 1), the equilibrium binding capacity at pH 5 as a function of the solution conductivity as evaluated from

static adsorption experiments (dashed curve in Figure 4, interpolated between the experimental values as needed), and the protein charge calculated from the known amino acid sequence. The values of the other parameters are as given in Table I. The only adjustable parameter in the model was β, which describes the contribution of the base resin to the effective surface charge density of the pore wall after protein adsorption (Eq. 11). For $\beta = 0.6$ and for the flow rate examined in this study, the calculated values of the dynamic-binding capacity are essentially equal to the static (equilibrium) binding capacity. The rate of pore diffusion is relatively rapid under these conditions since: (1) the model predicts that the pore wall retains a negative effective charge even after protein adsorption, and (2) the flow rate used in these experiments is relatively low (linear velocity of 100 cm/h). As β decreases, the effective charge on the pore wall becomes positive at low conductivities (i.e., at high equilibrium binding capacities), leading to significant electrostatic repulsion at the entrance to the pore. This causes the dynamic-binding capacity to pass through a maximum and then decrease at low conductivity, consistent with the experimental observations. This effect is quite dramatic at $\beta = 0.2$, with the maximum value of the dynamic-binding capacity being about 40 mg/mL while the static binding capacity is greater than 200 mg/mL at low conductivities. The best-fit value of β for this set of data was $\beta = 0.37$ (determined simply by eye), which is slightly smaller than the value determined for the batch uptake experiments ($\beta = 0.44$ in Fig. 2). This small discrepancy may simply reflect small differences in the conditions or resin samples used in these experiments; the equilibrium (static) binding capacity for the batch and column experiments at pH 5 and 5 mS/cm did differ by about 15%.

Figure 5 shows data for the dynamic-binding capacity as a function of the solution conductivity at pH 4, 5, and 6 (Harinarayan et al., 2006). In each case, the dynamic-binding capacity goes through a maximum at an intermediate conductivity, with the location of the maximum shifting to lower conductivity as the pH increases.

The solid curves in Figure 5 are the model calculations using $\beta = 0.53$, 0.37, and 0.18 for pH 4, 5, and 6, respectively, with these values determined by minimizing the sum of the squared residuals between the model and data. All the calculations were performed using the same pore size distribution, with the protein charge evaluated from the amino acid sequence and the static (equilibrium) binding capacity evaluated from an independent set of experiments (with interpolation between data at different conductivities using a polynomial fit to the data). The model calculations accurately capture the initial increase in dynamic-binding capacity as the solution conductivity is reduced, with this behavior directly attributable to the increase in the equilibrium capacity associated with the increased binding at lower salt concentrations. The model also captures the reduction in the dynamic-binding capacity at low conductivities, which is a direct result of the strong steric and electrostatic exclusion of the monoclonal antibody from the pores of the resin associated with the charge-reversal that occurs upon binding of the positively charged protein to the negatively charged resin. This electrostatic exclusion is much more pronounced at pH 4 due to the greater charge on the protein ($Z = 107$ at pH 4 compared to $Z = 57$ at pH 5 and 35 at pH 6). The maximum in the dynamic-binding capacity occurs very close to the point of charge-reversal for the pore walls; at low conductivities the pore wall is positively charged due to the large equilibrium protein binding, but the pore wall remains negative at high conductivity since the equilibrium binding capacity is relatively low under these conditions (Eq. 11).

The best-fit values of β have been plotted in Figure 6 as a function of the reciprocal of the protein charge ($1/Z$). The data are highly linear when plotted in this fashion, with

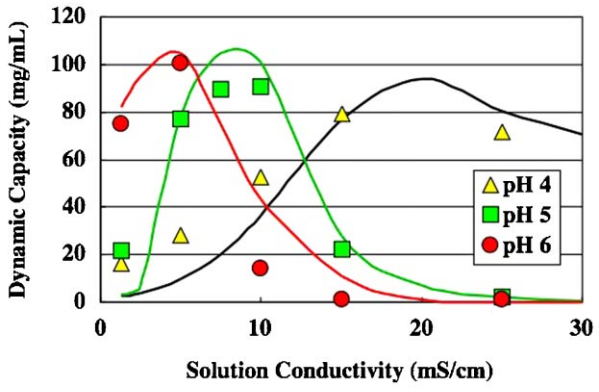

Figure 5. Dynamic-binding capacity of a monoclonal antibody as a function of solution conductivity at pH 4, 5, and 6. Solid curves are model calculations as described in the text. [Color figure can be seen in the online version of this article, available at www.interscience.wiley.com.]

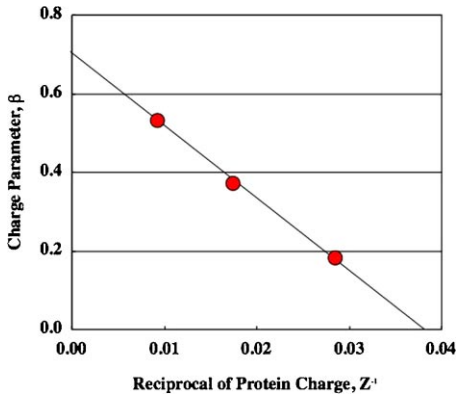

Figure 6. Best-fit values of the charge parameter β as a function of the reciprocal of the protein charge. Solid line is linear regression fit to the data with $r^2 = 0.999$. [Color figure can be seen in the online version of this article, available at www.interscience.wiley.com.]

$r^2 = 0.999$ for a simple linear regression. Although there is no theoretical basis for this dependence of the charge parameter on Z, the strong correlation given in Figure 6 suggests that it may be possible to estimate β at different pH values based on data at only a small number of pH, providing an opportunity to perform global simulations to estimate the dynamic-binding capacity as a function of both solution pH and conductivity.

Discussion

The theoretical model developed in this study provides the first quantitative analysis that is able to describe the observed maximum in the dynamic-binding capacity with solution conductivity. The model accounts for protein diffusion into the porous resin, with the partition coefficient at the pore entrance determined by the steric–electrostatic interactions between the charged protein and the charged surface of the pore. The high equilibrium binding capacity at low conductivities causes a reversal of the effective surface charge, leading to a strong electrostatic exclusion of the protein from the pore under these conditions. The net result is the anomalous ion exchange behavior where there is a reduction in the dynamic-binding capacity at low conductivities (at fixed pH) and at low pH (at fixed but relatively low values of the conductivity).

It is important to recognize that the model developed in this study is very approximate. It completely neglects any electrokinetic effects, it ignores the possibility of surface diffusion and any change in effective pore size due to collapse of the grafted dextran, and the approach used to evaluate the dynamic-binding capacity is unable to account for the detailed breakthrough behavior or the passage of the concentration front through the chromatographic column. However, the good agreement between the model calculations and experimental data provides a strong indication that the steric/electrostatic phenomenon, which was the primary focus of this theoretical analysis, provides the dominant mechanism for the unusual chromatographic behavior observed by Harinarayan et al. (2006) and Faude et al. (2007) for ion exchange of antibodies. In addition, this model framework may provide a means for estimating optimal conditions for ion exchange chromatography based on experimental measurements of the resin pore size distribution and the equilibrium (static) binding capacity along with an appropriate correlation for β, which describes the contribution of the resin charge to the effective surface charge density of the pore wall after protein binding. The results presented in Figure 6 show a very strong linear dependence of β on the inverse of the protein charge ($1/Z$), indicating that the more heavily charged proteins have less affect on the effective surface charge density (after protein binding) than would be expected based on the charge of the protein. This may be due to a charge regulation phenomenon. The binding of the very positively charged proteins would be expected to cause an exclusion of H^+ ions from the resin pores, leading to an increase in solution pH and a corresponding reduction in the effective surface charge on the pore walls (Ebersold and Zydney, 2004). Additional work would be needed to develop a more quantitative method for estimating the parameter β from independent measurements of the charge regulation phenomenon in this type of ion exchange system.

The authors acknowledge discussion and experimental support from Anders Ljunglöf, James Van Alstine, and Gunnar Malmquist of GE Healthcare Biosciences, Uppsala, Sweden. Fractogel is a registered trademark of Merck, Darmstadt. Sepharose, ÄKTA, and MultiTemp are trademarks of GE Healthcare companies. GE is a trademark of General Electric. Toyopearl is a trademark of TOSOH Bioscience, a member of the TOSOH Group.

References

Bungay PM, Brenner H. 1973. The motion of a closely fitting sphere in a fluid filled tube. Intl J Multiphase Flow 1:25–56.

Burns DB, Zydney AL. 2001. Contributions to electrostatic interactions on protein transport in membrane systems. AIChE J 47:1101–1114.

de la Torre JG, Carrasco B. 2002. Hydrodynamic properties of rigid macromolecules composed of ellipsoidal and cylindrical subunits. Biopolymers 63:163–167.

Dziennik SR, Belcher EB, Barker GA, DeBergalis MJ, Fernandez SE, Lenhoff AM. 2003. Non-diffusive mechanisms enhance protein uptake rates in ion exchange particles. Proc Natl Acad Sci 100:420–425.

Ebersold MF, Zydney AL. 2004. Separation of protein charge variants by ultrafiltration. Biotechnol Prog 20:543–549.

Faude A, Zacher D, Muller E, Bottinger H. 2007. Fast determination of conditions for maximum dynamic binding capacity in cation-exchange chromatography of human monoclonal antibodies. J Chromatogr A 1161:29–35.

Grimes BA, Liapis AI. 2002. The interplay of diffusional and electrophoretic transport mechanisms of charged solutes in the liquid film surrounding charged non-porous adsorbent particles employed in finite bath adsorption systems. J Colloid Interface Sci 248:504–520.

Hagel L. 1988. Gel filtration. In: Janson JC, Ryden LG, editors. Protein purification—Principles, high-resolution methods, and applications. New York: Wiley-VCH. pp. 79–145.

Harinarayan C, Mueller J, Ljunglof A, Fahrner R, Van Alstine J, van Reis R. 2006. An exclusion mechanism in ion exchange chromatography. Biotechnol Bioeng 95:775–787.

Hubbuch J, Linden T, Knieps E, Ljunglof A, Thommes J, Kula M-R. 2003. Mechanism and kinetics of protein transport in chromatography media studied by confocal laser scanning microscopy. Part I. The interplay of sorbent structure and fluid phase conditions. J Chromatogr A 1021: 93–104.

Johnson EM, Berk DA, Jain RK, Deen WM. 1995. Diffusion and partitioning of proteins in charged agarose gels. Biophys J 68:1561–1568.

Liapis AI, Grimes BA, Lacki K, Neretnieks I. 2001. Modeling and analysis of the dynamic behavior of mechanisms that result in the development of inner radial humps in the concentration of a single adsorbate in the adsorbed phase of porous adsorbent particles observed in confocal scanning laser microscopy experiments: Diffusional mass transfer and adsorption in the presence of an electrical double layer. J Chromatogr A 921:135–145.

Ljunglöf A, Lacki KM, Mueller J, Harinarayan C, van Reis R, Fahrner R, Van Alstine JM. 2007. Ion exchange chromatography of antibody fragments. Biotechnol Bioeng 96:515–524.

Mehta A, Zydney AL. 2006. Effect of membrane charge on flow and protein transport during ultrafiltration. Biotechnol Prog 22:484–492.

Pujar NS, Zydney AL. 1994. Electrostatic and electrokinetic interactions during protein transport through narrow pore membranes. Ind Eng Chem Res 33:2473–2482.

Pujar NS, Zydney AL. 1997. Charge regulation and electrostatic interactions for a spherical particle in a cylindrical pore. J Colloid Interface Sci 192:338–349.

Pujar NS, Zydney AL. 1998. Electrostatic effects on protein partitioning in size exclusion chromatography and membrane ultrafiltration. J Chromatogr A 796:229–238.

Smith FG, Deen WM. 1980. Electrostatic double-layer interactions for spherical colloids in cylindrical pores. J Colloid Interface Sci 78:444–465.

Stone MC, Carta G. 2007. Protein adsorption and transport in agarose and dextran-grafted agarose media for ion exchange. J Chromatogr A 1146: 202–215.

Teske CA, von Lieres E, Schroder M, Ladiwala A, Cramer SM, Hubbuch JJ. 2006. Competitive adsorption of labeled and native protein in confocal lasaer scanning microscopy. Biotechnol Bioeng 96:58–66.

Yamaguchi K, Hachiya K, Moriyama Y, Takeda K. 1996. Electrophoretic light scattering study of sodium dextran sulfate-lysozyme complex. J Colloid Interface Sci 179:249–254.

Yamamoto K, Hachiya K, Takeda K. 1992. Kinetic study of ion exchange reaction between lysozyme and carboxymethyl Sephadex C-25. Colloid Polym Sci 270:878–884.

Zhang SP, Sun Y. 2002. Study on protein adsorption kinetics to a dye-ligand adsorbent by the pore diffusion model. J Chromatogr A 964:35–46.

Zydney AL, Aimar P, Meireles M, Pimbley JM, Belfort G. 1994. Use of the log-normal probability density function to analyze membrane pore size distributions: Functional forms and discrepancies. J Membr Sci 91:293–298.